Room-temperature superfluidity in a polariton condensate

Giovanni Lerario[1], Antonio Fieramosca[1,2], Fábio Barachati[3], Dario Ballarini[1]*,
Konstantinos S. Daskalakis[4], Lorenzo Dominici[1], Milena De Giorgi[1], Stefan A. Maier[5],
Giuseppe Gigli[1,2], Stéphane Kéna-Cohen[3]* and Daniele Sanvitto[1,6]*

Superfluidity—the suppression of scattering in a quantum fluid at velocities below a critical value—is one of the most striking manifestations of the collective behaviour typical of Bose–Einstein condensates[1]. This phenomenon, akin to superconductivity in metals, has until now been observed only at prohibitively low cryogenic temperatures. For atoms, this limit is imposed by the small thermal de Broglie wavelength, which is inversely related to the particle mass. Even in the case of ultralight quasiparticles such as exciton-polaritons, superfluidity has been demonstrated only at liquid helium temperatures[2]. In this case, the limit is not imposed by the mass, but instead by the small binding energy of Wannier–Mott excitons, which sets the upper temperature limit. Here we demonstrate a transition from supersonic to superfluid flow in a polariton condensate under ambient conditions. This is achieved by using an organic microcavity supporting stable Frenkel exciton-polaritons at room temperature. This result paves the way not only for tabletop studies of quantum hydrodynamics, but also for room-temperature polariton devices that can be robustly protected from scattering.

First observed in liquid helium below the lambda point, superfluidity manifests itself in a number of fascinating ways. In the superfluid phase, helium can creep up along the walls of a container, boil without bubbles, or even flow without friction around obstacles. As early as 1938, Fritz London suggested a link between superfluidity and Bose–Einstein condensation (BEC)[3]. Indeed, superfluidity is now known to be related to the finite amount of energy needed to create collective excitations in the quantum liquid[4–7], and the link proposed by London was further evidenced by the observation of superfluidity in ultracold atomic BECs[1,8]. A quantitative description is given by the Gross–Pitaevskii (GP) equation[9,10] (see Methods) and the perturbation theory for elementary excitations developed by Bogoliubov[11]. First derived for atomic condensates, this theory has since been successfully applied to a variety of systems, and the mathematical framework of the GP equation naturally leads to important analogies between BEC and nonlinear optics[12–14]. Recently, it has been extended to include condensates out of thermal equilibrium, like those composed of interacting photons or bosonic quasiparticles such as microcavity exciton-polaritons and magnons[14,15]. In particular, for exciton-polaritons, the observation of many-body effects related to condensation and superfluidity such as the excitation of quantized vortices, the formation of metastable currents and the suppression of scattering from potential barriers[2,16–20] have

shown the rich phenomenology that exists within non-equilibrium condensates. Polaritons are confined to two dimensions and the reduced dimensionality introduces an additional element of interest for the topological ordering mechanism leading to condensation, as recently evidenced in ref. 21. However, until now, such phenomena have mainly been observed in microcavities embedding quantum wells of III–V or II–VI semiconductors. As a result, experiments must be performed at low temperatures (below ∼20 K), beyond which excitons autoionize. This is a consequence of the low binding energy typical of Wannier–Mott excitons. Frenkel excitons, which are characteristic of organic semiconductors, possess large binding energies that readily allow for strong light–matter coupling and the formation of polaritons at room temperature. Remarkably, in spite of weaker interactions as compared to inorganic polaritons[22], condensation and the spontaneous formation of vortices have also been observed in organic microcavities[23–25]. However, the small polariton–polariton interaction constants, structural inhomogeneity and short
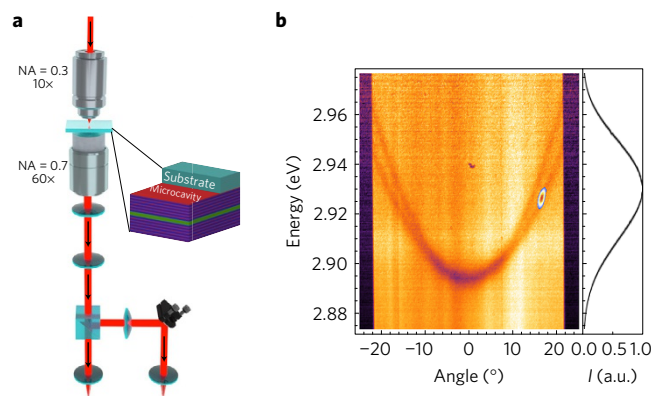
Figure 1 | Optical set-up and sample dispersion. a, Sketch of the optical set-up. The microcavity is placed between two microscope objectives and the excitation (35 fs pulsed laser) is incident from the substrate side, while detection is performed from the microcavity deposition side.
b, Energy–angle map of the microcavity under white light illumination superimposed with the transmitted signal under resonant laser excitation (the transparency threshold is set at 50% of the maximum intensity). The incidence angle can be related to the in-plane wavevector using $k_{\parallel} = (\omega/c)\sin\theta$ where ω is the angular frequency, c is the speed of light in vacuum and θ is the angle of incidence. The energy spectrum of the excitation laser is shown on the right.

[1]CNR NANOTEC Institute of Nanotechnology, via Monteroni, 73100 Lecce, Italy. [2]Dipartimento di matematica e fisica "Ennio De Giorgi", Università del Salento, Via Arnesano, 73100 Lecce, Italy. [3]Department of Engineering Physics, École Polytechnique de Montréal, Montréal, Québec H3C 3A7, Canada. [4]COMP Centre of Excellence, Department of Applied Physics, Aalto University, PO Box 15100, Fi-00076 Aalto, Finland. [5]Department of Physics, Imperial College London, London SW7 2AZ, UK. [6]INFN, Sez. di Lecce, 73100 Lecce, Italy. *e-mail: dario.ballarini@gmail.com; s.kena-cohen@polymtl.ca; daniele.sanvitto@nanotec.cnr.it
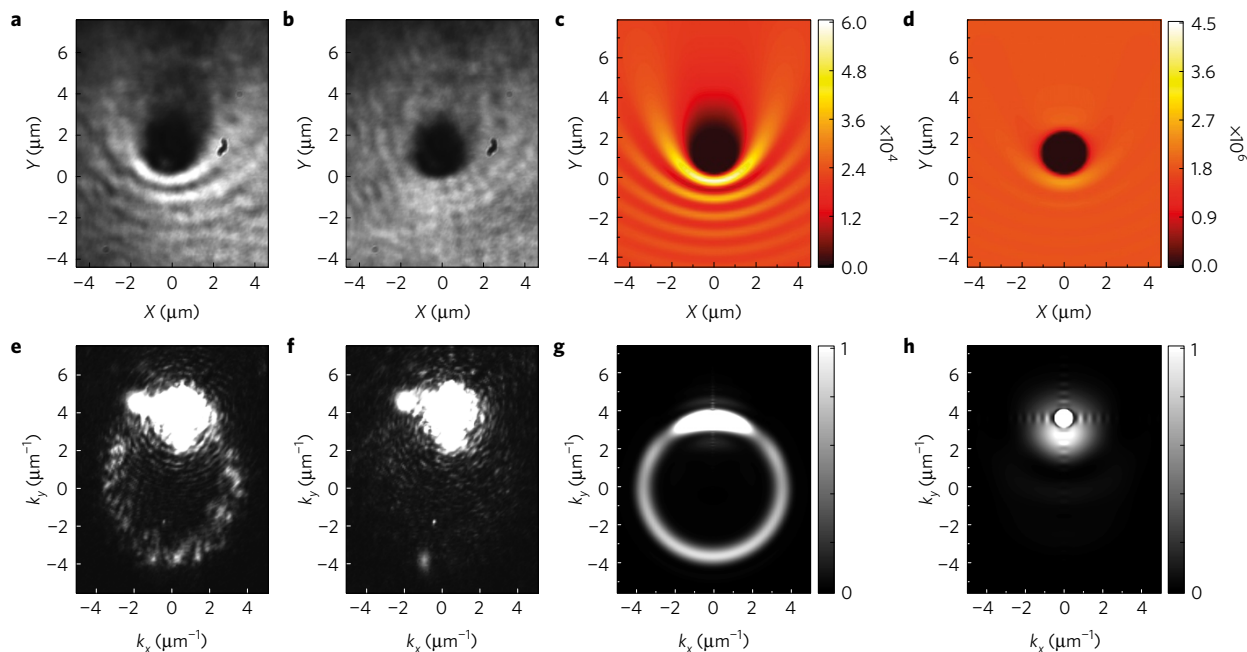
Figure 2 | Superfluid behaviour. a, Real-space polariton distribution for flow with group velocity of 19 μm ps^{-1} from the bottom to the top of the image across an artificial defect. The Gaussian pump, with a full-width at half-maximum (FWHM) of 13 μm, is centred 2 μm below the defect position. The polariton density is 0.5×10^6 pol μm^{-2}. **b**, Real-space intensity distribution at a polariton density of 10^7 pol μm^{-2}. The interference fringes and the shadow cone beyond the defect vanish almost perfectly, revealing the physics of a fluid with zero viscosity. **c,d**, The corresponding time-averaged calculation is shown for the supersonic (low density) (**c**) and superfluid (**d**) regimes at pump powers corresponding to peak polariton densities of 1.6×10^5 pol μm^{-2} and 2.4×10^7 pol μm^{-2}, respectively. The colour scale corresponds to the average polariton density during the 800 fs integration interval. **e**, Saturated image in momentum space corresponding to **a**; the elastic scattering ring generated by the presence of the defect is clearly observable. **f**, Saturated image in momentum space corresponding to **b**; the elastic scattering ring is completely suppressed at high polariton densities. **g,h**, Corresponding calculated momentum-space density profiles, also showing the disappearance of the Rayleigh scattering ring pattern in the superfluid regime.

lifetimes in these structures have until now prevented the observation of behaviour directly related to the quantum fluid dynamics (such as superfluidity). In this work, we show that superfluidity can indeed be achieved at room temperature and this is, in part, a result of the much larger polariton densities attainable in organic microcavities, which compensate for their weaker nonlinearities.

Our sample consists of an optical microcavity composed of two dielectric mirrors surrounding a thin film of 2,7-Bis[9,9-di (4-methylphenyl)-fluoren-2-yl]-9,9-di(4-methylphenyl)fluorene (TDAF) organic molecules. Light–matter interaction in this system is so strong that it leads to the formation of hybrid light–matter modes (polaritons), with a Rabi energy $2\Omega_R \sim 0.6$ eV. A similar structure has been used previously to demonstrate polariton condensation under high-energy non-resonant excitation[24]. Upon resonant excitation, it allows for the injection and flow of polaritons with a well-defined density, polarization and group velocity.

The experimental configuration is shown in Fig. 1a. The sample is positioned between two microscope objectives to allow for measurements in a transmission geometry while maintaining high spatial resolution. A polariton wavepacket with a chosen wavevector is created by exciting the sample with a linearly polarized 35 fs laser pulse resonant with the lower polariton branch (see Methods). By detecting the reflected or transmitted light using a spectrometer and a charge-coupled device (CCD) camera, energy-resolved space and momentum maps can be acquired. An example of the experimental polariton dispersion under white light illumination is shown in Fig. 1b. The parabolic TE- and TM-polarized lower polariton branches appear as dips in the reflectance spectra. The figure also shows an example of how the laser energy, momentum and polarization can be precisely tuned to excite, in this case, the TE lower polariton branch at a given angle. The resonantly excited polariton state is shown as a transmission spot superimposed on

the reflectance map. Note the spectral filtering created by the microcavity itself on the ultrashort pump pulse, shown on the right of Fig. 1b. In contrast to experiments on superfluidity in atomic condensates[1,8], the position of the defect is kept fixed in space in our experiments, while the speed of the quasiparticle flow is controlled by using the excitation angle. This speed is directly related to the polariton group velocity $v_g = \hbar k_p/m_{LP}$, where $\hbar$ is the reduced Planck constant, k_p is the polariton wavevector and m_{LP} the effective mass. This scheme is very closely related to the original proposal for superfluidity in nonlinear microcavities[13] and to the proposal for polariton superfluidity in ref. 15 realized in ref. 2. In the latter, the behaviour depends critically on the energetic detuning between the pump and the polariton dispersion, which is renormalized by polariton–polariton interactions. In our experiments, the broadband impulsive pump ensures that the polariton density is always dominated by the spectral component of the pump which is resonant with the renormalized dispersion.

Figure 2 shows the time-averaged transmitted (panels a,b) and scattered (panels e,f) intensities for a polariton flow moving upwards across an obstacle with an exciting angle chosen such that the flow speed is 19 μm ps^{-1}. The point defect, which serves as the obstacle, was artificially created by focusing and increasing the laser intensity beyond the sample damage threshold. We find that at low polariton densities, the defect causes polaritons to scatter to isoenergetic states possessing the same wavevector magnitude; a phenomenon known as Rayleigh scattering. This can be observed as a bright elastic scattering ring in momentum space (Fig. 2e) and a modulation in real-space characteristic of supersonic flow, shown here for a polariton density of approximately 0.5×10^6 pol μm^{-2}. The scattered polaritons interfere with the incoming flow, generating the spatial pattern of fringes visible in Fig. 2a. Meanwhile, in the wake of the artificial defect a shadow cone appears due to the reduced
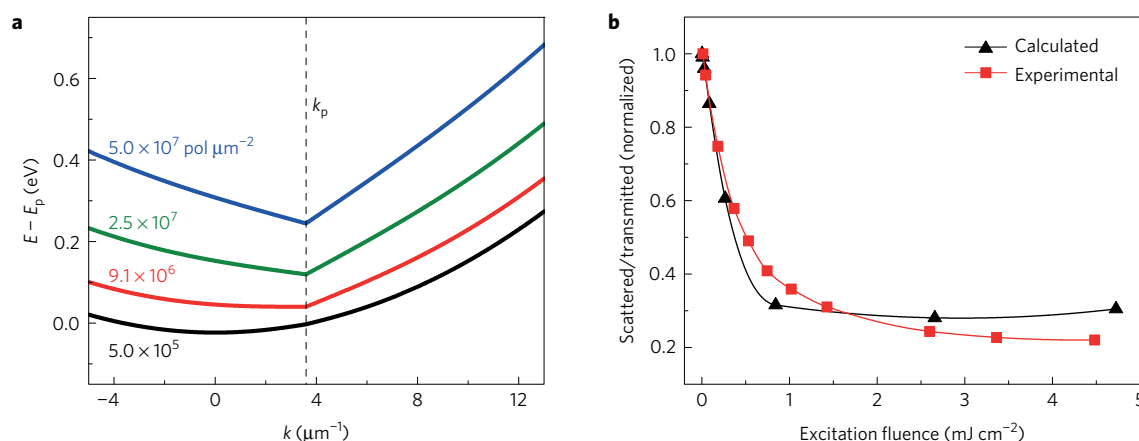
Figure 3 | Excitation spectrum and power dependence. a, Positive Bogoliubov branch as a function of polariton density (see Supplementary Information for details). At high polariton densities, the linearized dispersion becomes apparent. Note the absence of elastic scattering beyond 9.1×10^6 pol μm^{-2}. **b**, Calculated and experimental ratio of the scattered light to transmitted light obtained from the Rayleigh scattering patterns. Both the absolute and relative scattering are suppressed in the superfluid regime. Note that the precise shape of these curves is sensitive to the choice of k-space mask used to block the transmitted light.

transmission across the defect. When the pump power is increased such that the polariton density reaches values close to 10^7 pol μm^{-2}, the shadow cone and the waves upstream vanish almost completely, as expected for a superfluid. This is confirmed by the image in momentum space (Fig. 2f), in which the scattering ring disappears almost fully. By solving the time-dependent GP equation, we can calculate the polariton evolution using parameters corresponding to our experimental conditions (see Methods). To compare with the experimental time-integrated images, the calculated polariton density, $|\psi(\mathbf{r}, t)|^2$, was integrated over a time interval of 800 fs and is shown in Fig. 2c,d. In the low-density supersonic regime (Fig. 2c), the calculation reproduces the characteristic features of the experiment (Fig. 2a), such as the parabolic density modulation in front of the defect, which results from interference between incident and scattered waves, and the shadow behind the defect. Figure 2d shows the case where the incident fluence is increased such that the peak polariton density reaches 2.4×10^7 pol μm^{-2}, corresponding to the subsonic regime: that where the condensate exhibits superfluid flow. Here, scattering by the defect is visibly suppressed. As in the experiment (Fig. 2b), some interference fringes around the defect remain slightly visible. This is a consequence of time integration, which includes periods during the pulse where polariton densities remain in the supersonic regime. Time-resolved snapshots in both regimes are shown in Supplementary Figs 4 and 5.

Although there is no stationary state in the pulsed case, we can nevertheless make a link with the renormalized polariton dispersion, which depends instantaneously on density, as shown in Fig. 3a. As the density is increased, the dispersion relation blueshifts and is linearized with a slope related to the sound speed (see Supplementary Information). Beyond 9×10^6 pol μm^{-2}, the sound speed for elementary excitations of the fluid becomes larger than the flow velocity, and elastic scattering is suppressed (note the absence of isoenergetic states at the resonant pump energy). Figure 3b shows the measured and calculated reduction in scattering obtained from the Rayleigh scattering patterns as a function of the pump fluence. As the polariton density is increased, we find a reduction in both the absolute and relative amounts of scattering, until finally the subsonic condition is satisfied.

A homodyne interferometric technique similar to that in ref. 18 was used to probe the time-evolution of the polariton fluid with a resolution of a few tens of femtoseconds (see Methods). Here, the emission is made to interfere with an expanded reference of constant phase derived from the laser pulse[26]. This allows us to

extract spatially resolved information related to the density and the phase of the polariton fluid. The latter allows us to identify phase dislocations due to quantized vortices. In Fig. 4, snapshots at the instant of maximum polariton density are shown in the supersonic and superfluid regimes (left and right columns, respectively). In the supersonic regime, a vortex–antivortex pair is dynamically generated behind the defect and the vortex cores are visible as two density minima (indicated by a square and a circle in Fig. 4a). They are also easily identified in the phase map of Fig. 4c due to the distinctive 2π phase rotation around the vortex cores. The time-resolved density in momentum space can be extracted by Fourier-transforming the interferograms, and is shown in Fig. 4e,f. As in the time-integrated images, the elastic ring in momentum space and the density modulations are fully suppressed in the superfluid regime. In our experiments, the condensate phase is initially imprinted by the laser pulse, but pulsed excitation can be used to reveal the proliferation of vortex pairs after excitation when the density drops below the superfluid threshold. The ability to observe the out-of-equilibrium dynamics is an important advantage of our configuration over previous demonstrations of polariton superfluidity at 4 K, which used steady-state resonant excitation[2] or the perturbation of the parametric process (TOPO)[27]. In the case of resonant excitation, phase stiffness is imposed by the continuous wave laser, and the presence of more than one condensed state in the TOPO case[28] complicates the interpretation of the temporal dynamics. Our experiment allows for the vortex dynamics after the pulse to be studied (see videos in Supplementary Information).

Finally, to test the effect of the polariton group velocity on the superfluid behaviour, we have repeated the experiments shown in Fig. 2, but for different resonant excitation conditions along the polariton dispersion. When the group velocity is lowered, the superfluid behaviour is preserved. However, when the velocity is increased to 27 μm ps^{-1}, superfluid behaviour is no longer achievable in the range of polariton densities attainable below the damage threshold of our sample. This can be seen in Fig. 5, where the shadow cone remains visible at both low and high densities.

In conclusion, we have experimentally demonstrated the superfluid flow of polaritons around a defect in an organic microcavity under ambient conditions. Strikingly, the perturbations induced by artificial and natural potential barriers on the polariton flow vanish for high enough particle densities and low group velocities (see Supplementary Information). In agreement with the experimental results, GP calculations show that despite the small
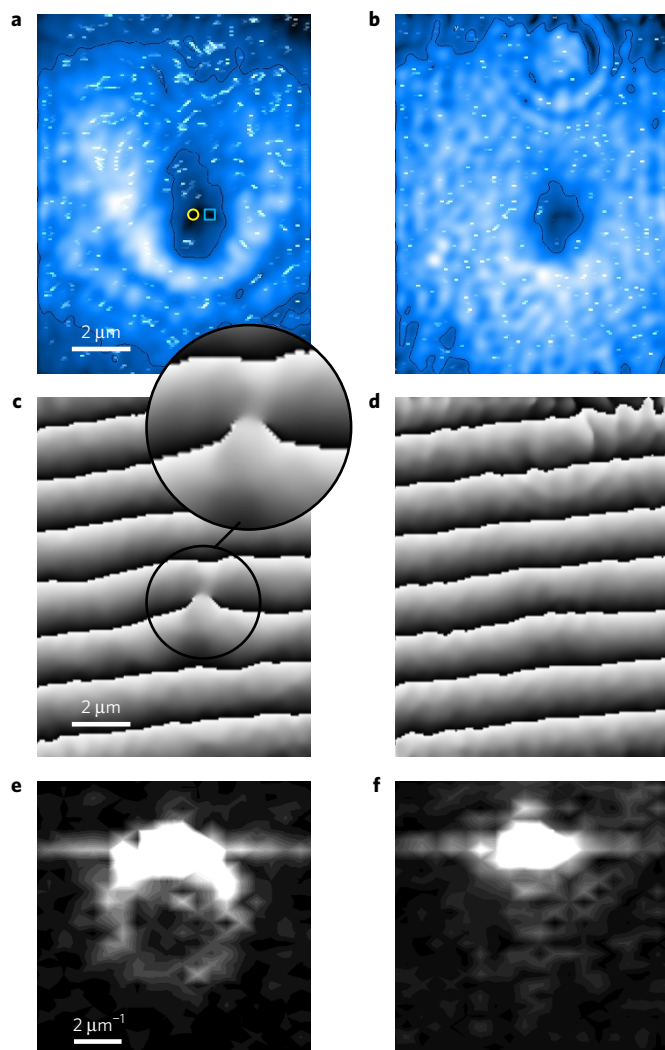
Figure 4 | Time-resolved interferograms. Time-resolved snapshots of the real-space (**a**,**b**), phase (**c**,**d**) and momentum-space (**e**,**f**) patterns retrieved from interferograms at the instant where the polariton density is highest for the supersonic (**a**,**c**,**e**) and superfluid (**b**,**d**,**f**) regimes. Vortex and antivortex positions are indicated as a circle and a square in the density map in **a**. These correspond to the phase dislocations highlighted in the phase map. In the superfluid regime, the elastic scattering ring, the interference pattern in front of the defect, the dark cone in the wake of the defect and the vortex–antivortex pair are suppressed.

polariton–polariton interaction constant of organic polaritons, the superfluid regime at a group velocity of 19 μm ps^{-1} is achieved when the polariton density is increased to approximately 10^7 pol μm^{-2}. The observation of superfluid behaviour at room temperature may have important implications for the realization of photonic devices protected from scattering by means of polariton–polariton interactions. It is worth noting that in polariton condensates under resonant excitation, a definition of the superfluid fraction, which is the part of the fluid that responds only to irrotational (non-transverse) forces, is still an open and important question[29]. In this context, the short pulse excitation used in the present experiment is particularly useful, because it could allow for spatially separated excitation in samples with longer polariton lifetimes. The intermediate pulse length regime is also of interest as it would allow for the observation of quasi-steady-state behaviour free of transients and relaxation oscillations at early times (see Supplementary Fig. 6 for predicted behaviour). Under this configuration, single-shot measurements could allow the observation of free vortex formation
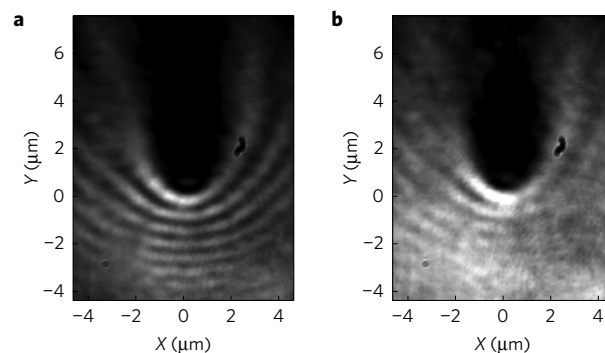

Figure 5 | Influence of the polariton group velocity. Real-space intensity profiles for polariton flow (from the bottom to the top of the images) across the same artificial defect as in Fig. 2 when the polariton group velocity is increased to 27 μm ps^{-1}. The densities are kept the same: 0.5×10^6 pol μm^{-2} (**a**) and 10^7 pol μm^{-2} (**b**). As in Fig. 2, the system is in the supersonic regime at low densities, which is evidenced by the fringes in front of the defect and the shadow cone in **a**. Because of the increased velocity, however, the flow remains supersonic even at the highest density, in agreement with theory.

for suitable conditions of the barrier potential and fluid density, opening the way to the study of hydrodynamic effects in quantum fluids in room-temperature tabletop experiments.

Methods

Methods, including statements of data availability and any associated accession codes and references, are available in the online version of this paper.

References

1. Onofrio, R. *et al*. Observation of superfluid flow in a Bose-Einstein condensed gas. *Phys. Rev. Lett.* **85,** 2228–2231 (2000).
2. Amo, A. *et al*. Superfluidity of polaritons in semiconductor microcavities. *Nat. Phys.* **5,** 805–810 (2009).
3. London, F. The λ-phenomenon of liquid helium and the Bose-Einstein degeneracy. *Nature* **141,** 643–644 (1938).
4. Allen, J. F. & Misener, A. D. Flow of liquid helium II. *Nature* **141,** 75 (1938).
5. Kapitza, P. Viscosity of liquid helium below the λ-point. *Nature* **141,** 74 (1938).
6. Landau, L. Theory of the superfluidity of helium II. *Phys. Rev.* **60,** 356–358 (1941).
7. Landau, L. On the theory of superfluidity. *Phys. Rev.* **75,** 884–885 (1949).
8. Desbuquois, R. *et al*. Superfluid behaviour of a two-dimensional Bose gas. *Nat. Phys.* **8,** 645–648 (2012).
9. Gross, E. P. Structure of a quantized vortex in boson systems. *Il Nuovo Cimento* **20,** 454–477 (1961).
10. Pitaevskii, L. P. Vortex lines in an imperfect Bose gas. *Sov. Phys. JETP* **13,** 451–454 (1961).
11. Pitaevskii, L. P. & Stringari, S. *Bose-Einstein Condensation* (No. 116 in Oxford Science Publications, Clarendon Press, 2003).
12. Chiao, R. Y. & Boyce, J. Bogoliubov dispersion relation and the possibility of superfluidity for weakly interacting photons in a two-dimensional photon fluid. *Phys. Rev. A* **60,** 4114–4121 (1999).
13. Bolda, E. L., Chiao, R. Y. & Zurek, W. H. Dissipative optical flow in a nonlinear Fabry–Pérot cavity. *Phys. Rev. Lett.* **86,** 416–419 (2001).
14. Carusotto, I. & Ciuti, C. Quantum fluids of light. *Rev. Mod. Phys.* **85,** 299–366 (2013).
15. Carusotto, I. & Ciuti, C. Probing microcavity polariton superfluidity with resonant Rayleigh scattering. *Phys. Rev. Lett.* **93,** 166401 (2004).
16. Lagoudakis, K. G. *et al*. Quantized vortices in an exciton–polariton condensate. *Nat. Phys.* **4,** 706–710 (2008).
17. Sanvitto, D. *et al*. Persistent currents and quantized vortices in a polariton superfluid. *Nat. Phys.* **6,** 527–533 (2010).
18. Nardin, G. *et al*. Hydrodynamic nucleation of quantized vortex pairs in a polariton quantum fluid. *Nat. Phys.* **7,** 635–641 (2011).

19. Sanvitto, D. *et al*. All-optical control of the quantum flow of a polariton condensate. *Nat. Photon.* **5,** 610–614 (2011).
20. Amo, A. *et al*. Polariton superfluids reveal quantum hydrodynamic solitons. *Science* **332,** 1167–1170 (2011).
21. Caputo, D. *et al*. Topological order and equilibrium in a condensate of exciton-polaritons. Preprint at http://arXiv.org/abs/1610.05737 (2016).
22. Lerario, G. *et al*. High-speed flow of interacting organic polaritons. *Light: Science & Applications* **6,** e16212 (2017).
23. Plumhof, J. D., Stöferle, T., Mai, L., Scherf, U. & Mahrt, R. F. Room-temperature Bose–Einstein condensation of cavity exciton-polaritons in a polymer. *Nat. Mater.* **13,** 247–252 (2013).
24. Daskalakis, K. S., Maier, S. A., Murray, R. & Kéna-Cohen, S. Nonlinear interactions in an organic polariton condensate. *Nat. Mater.* **13,** 271–278 (2014).
25. Daskalakis, K., Maier, S. & Kéna-Cohen, S. Spatial coherence and stability in a disordered organic polariton condensate. *Phys. Rev. Lett.* **115,** 035301 (2015).
26. Dominici, L. *et al*. Real-space collapse of a polariton condensate. *Nat. Commun.* **6,** 8993 (2015).
27. Amo, A. *et al*. Collective fluid dynamics of a polariton condensate in a semiconductor microcavity. *Nature* **457,** 291–295 (2009).
28. Berceanu, A. C. *et al*. Multicomponent polariton superfluidity in the optical parametric oscillator regime. *Phys. Rev. B* **92,** 035307 (2015).
29. Keeling, J. Superfluid density of an open dissipative condensate. *Phys. Rev. Lett.* **107,** 080402 (2011).

Author contributions

G.L. conceived and performed the optical measurements with assistance from A.F.; K.S.D. fabricated the sample and F.B. performed the simulations. G.L., D.B., F.B., K.S.D., S.K.-C. and D.S. co-wrote the manuscript. All authors contributed to the data analysis. S.K.-C. supervised the fabrication and simulation work and D.S. supervised the measurements and coordinated the project.

Additional information

Supplementary information is available in the online version of the paper. Reprints and permissions information is available online at www.nature.com/reprints. Publisher's note: Springer Nature remains neutral with regard to jurisdictional claims in published maps and institutional affiliations. Correspondence can be addressed to D.B., S.-K.C. or D.S. Requests for materials should be addressed to D.B.

Competing financial interests

The authors declare no competing financial interests.

Methods

Experiment. The microcavity under investigation is similar to that in ref. 25 and consists of a 130-nm-thick film of layer of TDAF sandwiched between two dielectric Bragg reflectors. The organic layer was thermally evaporated in vacuum and the mirrors, which are composed of nine pairs of alternating Ta_2O_5/SiO_2, sputtered in the same chamber. Tunable short pulse excitation was obtained using an optical parametric amplifier pumped by a Ti:sapphire regenerative amplifier at 10 kHz. Polaritons with a specific group velocity were created by focusing the laser on the back focal plane of the first microscope objective, which was a $60\times$ long working distance objective on the substrate side. The overall magnification for real space in detection was $300\times$ and the excitation spot was approximately 13 μm FWHM. Furthermore, we use a white light source incident from the detection side (in the reflectance configuration) to measure the polariton dispersion, facilitating resonant tuning of the excitation laser on the polariton branch. The FWHM of the excited momenta is $0.55\,\mu m^{-1}$ and the incident laser spectral width corresponds to a FWHM of 7.8 nm at $\lambda = 424$ nm. In all of the experiments, care is taken to ensure that after reaching the highest polariton density the initial condition is fully recovered after reducing the pump power to its initial value. This limits the incident fluence to approximately $4\,mJ\,cm^{-2}$ and short measurement intervals.

To obtain the time dynamics, we used pulsed resonant excitation and off-axis digital holography. This technique relies on the interference of the emission with a homodyne expanded reference beam with homogeneous density and phase profiles, implemented in a Mach–Zehnder configuration with precisely tunable delay line. The use of a digital fast Fourier transform (FFT) on the original interferograms allows one to retain only the information associated with a given time frame upon changing the delay of the reference pulse train. In such a way the two-dimensional maps of both the emission amplitude and phase can be obtained as a sequence of ultrafast snapshots. In the present case we used a time step of 20 fs. Each interferogram and retrieved snapshot results from hundreds of repeated events. For further details on the off-axis digital holography implementation see ref. 26.

Gross–Pitaevskii (GP) simulations. Because of the small interaction energy, as compared to the splitting between lower (LP) and upper polariton branches, it is sufficient to consider only the lower polariton field $\psi(\mathbf{r}, t)$. Its time-evolution is governed by a generalized GP equation

$$i\hbar \frac{\partial \psi(\mathbf{r}, t)}{\partial t} = \left[\hbar\omega_0 - \frac{\hbar^2 \nabla^2}{2m_{LP}} + V(\mathbf{r}) - \frac{i\hbar\gamma_{LP}}{2} + g|\psi(\mathbf{r}, t)|^2 \right] \psi(\mathbf{r}, t) + \hbar P(\mathbf{r}, t) \quad (1)$$

The first two terms on the right-hand side correspond to a parabolic approximation for the lower polariton branch dispersion, which is valid under our experimental conditions. Here $\hbar\omega_0$ is the LP energy at $k = 0$, m_{LP} is the effective mass, $V(\mathbf{r})$ is the scattering defect potential, γ_{LP} is the lower polariton dissipation rate, g is the polariton–polariton interaction constant and $P(\mathbf{r}, t)$ is the driving term. The pump field is taken to be a plane wave modulated by a temporal Gaussian envelope

$$P(\mathbf{r}, t) = F_p e^{i(\mathbf{k}\cdot\mathbf{r} - \omega_p t)} e^{-\frac{(t - t_0)^2}{2\sigma_t^2}} \quad (2)$$

where σ_t can be related to the intensity FWHM using $\sigma_t = \text{FWHM}/(2\sqrt{\ln 2})$. The possible influence of chirp has been considered in the Supplementary Information and was found not to qualitatively affect the behaviour. The amplitude of the driving term can be related to the incident pump intensity using input–output theory[30] as

$$F_P = C_{k_p} \sqrt{\frac{\gamma_{LP} I_0}{2\hbar\omega_p}} \quad (3)$$

where $C_{k_p} = 0.88$ is the Hopfield coefficient for the photon fraction of the lower polariton branch at the pump wavevector k_p. For simplicity, the defect is taken to be an infinite barrier with vanishing boundary conditions. The remaining simulation parameters are $\hbar\omega_0 = 2.896$ eV, $m_{LP} = 1.976 \times 10^{-35}$ kg, $\gamma_{LP} = 10^{13}\,s^{-1}$, $g = 5 \times 10^{-3}\,\mu eV\,\mu m^2$, $\mathbf{k}_p = 3.59\,\hat{y}\,\mu m^{-1}$ and $\hbar\omega_p = 2.9242$ eV.

To make a connection to the pump fluence, we can use $E_{in} = I_0 \sigma_t \sqrt{\pi}$, which gives $26.6\,mJ\,cm^{-2}$ for the incident fluence in the superfluid regime. This is comparable with the experimental value of $4\,mJ\,cm^{-2}$, given the approximations made in connection with input–output theory and the approximate value of the polariton interaction constant. Indeed, the latter is the only experimental parameter not known with certainty. The value chosen here is close to our previous estimate of $g = 10^{-3}\,\mu eV\,\mu m^2$ in this structure[25], and also to that obtained using the resonant blueshift at high powers (see Supplementary Information). At higher powers, however, the measured blueshift of the polariton may be strongly affected by the thermal load of the pump, causing a competing redshift of the polariton energy due to an expansion of the cavity length. A k-space mask of radius $4.8\,\mu m^{-1}$ centred on $\mathbf{k}_p$ was used to obtain Fig. 3b.

Data availability. The data that support the plots within this paper and other findings of this study are available from the corresponding authors upon reasonable request.

References

30. Wouters, M. & Carusotto, I. Parametric oscillation threshold of semiconductor microcavities in the strong coupling regime. *Phys. Rev. B* **75,** 075332 (2007).